Hindawi Publishing Corporation
International Journal of Rotating Machinery
Volume 2016, Article ID 5921463, 14 pages
http://dx.doi.org/10.1155/2016/5921463

Research Article

Vane Clocking Effects on Stator Suction Side Boundary Layers in a Multistage Compressor

Natalie R. Smith and Nicole L. Key

School of Mechanical Engineering, Purdue University, 500 Allison Road, West Lafayette, IN 47907, USA

Correspondence should be addressed to Nicole L. Key; nkey@purdue.edu

Received 29 December 2015; Accepted 14 April 2016

Academic Editor: Tariq Iqbal

Copyright © 2016 N. R. Smith and N. L. Key. This is an open access article distributed under the Creative Commons Attribution License, which permits unrestricted use, distribution, and reproduction in any medium, provided the original work is properly cited.

The stator inlet flow field in a multistage compressor varies in the pitchwise direction due to upstream vane wakes and how those wakes interact with the upstream rotor tip leakage flows. If successive vane rows have the same count, then vane clocking can be used to position the downstream vane in the optimum circumferential position for minimum vane loss. This paper explores vane clocking effects on the suction side vane boundary layer development by measuring the quasi-wall shear stress on the downstream vane at three spanwise locations. Comparisons between the boundary layer transition on Stator 1 and Stator 2 are made to emphasize the impact of rotor-rotor interactions which are not present for Stator 1 and yet contribute significantly to transition on Stator 2. Vane clocking can move the boundary layer transition in the path between the wakes by up to 24% of the suction side length at midspan by altering the influence of the Rotor 1 wakes in the 3/rev modulation from rotor-rotor interactions. The boundary layer near the vane hub and tip experiences earlier transition and separation due to interactions with the secondary flows along the shrouded endwalls. Flow visualization and Stator 2 wakes support the shear stress results.

1. Introduction

Blade row interactions in a multistage axial compressor affect stage performance, unsteady blade loading, and acoustic signatures. To computationally model blade row interactions, researchers have used body forces [1, 2], harmonic balancing [3], overset grids (Chimera method) [4, 5], and unsteady calculations with sliding planes [6, 7]. To determine the fidelity of such models, experimental data in multistage compressors are required to evaluate the relative contribution of upstream vane and blade rows.

Vane clocking is the circumferential indexing of successive vane rows with similar vane counts. Vane clocking affects stage efficiency [8–11], unsteady blade loading [12, 13], and acoustics [14–16]. In research facilities where vanes can be individually positioned, vane clocking is a useful tool to investigate blade row interactions. Many researchers have discussed clocking configurations where the upstream vane wake impinges on the downstream vane leading edge. While the circumferential position of the upstream wake with respect to the downstream vane is certainly affected by vane clocking, Smith et al. [17] also showed that the radial penetration of the tip leakage flow from the upstream rotor changed across the downstream stator pitch due to the interaction between the upstream vane wake and the upstream rotor tip leakage flow. Thus, the pitchwise variations in the flow field associated with vane clocking include not only the upstream vane wakes, but also differing rotor tip leakage flow structures.

The open literature shows the potential for changes in stage efficiency and effects on the downstream stator surface performance with different clocking configurations in compressors. The numerical studies of Gundy-Burlet and Dorney [18] were of the first compressor vane clocking studies to emerge and had findings similar to the turbine literature of a nearly sinusoidal variation between maximum and minimum clocking locations. Barankiewicz and Hathaway [8] measured small changes in overall loss coefficient with clocking in the NASA Four-Stage Axial Compressor Facility, but these differences were within the manufacturing and assembly tolerances of the compressor. Saren et al. [10] have published one of the few high-speed compressor clocking experimental

studies in the open literature, and the measured change in average stage efficiency was 1%, but local spanwise efficiency changes were as large as 7-8%. The computational study that accompanied these experiments showed that the leading edge wake impingement clocking configuration provided the maximum stage efficiency, in agreement with the turbine literature.

Recently, extensive studies of vane clocking have been performed in the Purdue 3-Stage Compressor Research Facility. After careful attention to measurement details, Key et al. [11] showed a measurable change in embedded stage efficiency at both design loading and high loading operating conditions. At design loading, the clocking effects were confined to 70–88% span, while at high loading, the entire spanwise total pressure distribution was affected by vane clocking. Smith and Key [19] explored many loading conditions and showed that there was a maximum clocking effect at high loading around 15% stall margin, and higher loading conditions experienced less clocking effects on vane loss. They also showed that clocking had a negligible impact on stall margin [20].

There have been studies [21] looking at the changes in the unsteady blade loading of the embedded rotor with vane clocking, in which case the downstream stator's potential fields play an important role along with the upstream stator wake. Some researchers [10, 22] have investigated changes in the downstream vane surface properties with vane clocking. The interaction from the upstream wakes, both the stator and rotor, influence the unsteady loading of the downstream stator. A computational study of a 1.5-stage turbine by Griffin et al. [23] found lower surface pressure unsteadiness along the stator suction surface was associated with the lower pressure loss clocking configuration. However, a study by Saren et al. [10] reported that the maximum efficiency clocking configuration had both more unsteadiness and higher frequency content. Recently, Smith and Key [24] showed the effects of rotor-rotor interactions on the unsteady vane loading over a rotor revolution. They showed that the mean surface pressure per blade pass period could change by 4% and the dynamic pressure response per blade pas period changed by 100% across a rotor revolution. Furthermore, changing the vane clocking configuration altered these interactions by up to 50%.

Since clocking changes the profile loss on the downstream vane, it is natural to investigate how clocking affects the vane's surface boundary layer. The researches [25–27] available in the open literature that discusses vane clocking effects on compressor boundary layer development are limited to low-speed, 1.5-stage, and/or repeating stage machines. Walker et al. [25] investigated suction side stator boundary layer transition in a single stage compressor consisting of an IGV-rotor-stator. They clocked the upstream IGV so that the IGV wake provided additional unsteadiness to the downstream vane and investigated changes in boundary layer transition. The work of Henderson et al. [26] examined the effects of clocking the IGV with the stator in their single stage compressor under different inlet turbulence levels. Their findings were consistent with previous work including those in turbines [28].

Therefore, this paper aims to explore the changes in boundary layer transition in a facility where vane clocking effects on the embedded stage performance have been well documented. This is done with unsteady hot film measurements acquired on the suction surface of the downstream vane row. Others have looked at this type of measurement in a compressor.

Mailach and Vogeler [29] investigated the boundary layer response on the first stage stator vane in a low-speed research compressor with results showing movement of the transition zone up to 80% of the chord due to wake-induced transition. Increasing loading from design point to near the stability limit shifted the onset of transition upstream and broadened the wake-induced paths. Halstead et al. [28] acquired shear stress data on the first and third rotor of a 4-stage low-speed research compressor featuring repeating stages. Thus, they were able to contrast results of boundary layers from the first rotor (without any upstream vane influence) with results from the third rotor which was influenced by several upstream vane rows and wakes. The 4-stage compressor featured repeating stages where the vane counts were identical for every stage, as were the rotor counts. Consequently, the contributions from the different upstream stages were difficult to discern because of the similar blade counts. Smith and Key [30] showed that the rotor-rotor interactions in a compressor without repeating stages could affect the completion of transition by 20% s. These studies further motivate the present investigation blade row interaction effects including vane clocking on the embedded stator boundary layer transition.

2. Experimental Methodology

This research was conducted in the Purdue 3-Stage Axial Compressor Research Facility [31]. This section will discuss details about the facility and compressor as well as the measurement techniques and analyses used.

2.1. Facility and Compressor Details. The compressor facility is an open circuit that draws atmospheric air through screens into a large settling chamber. A bell mouth directs the flow into the inlet ducting where it is metered by an ASME standard long-form venturi. A nosecone reduces the flow area to the 5.08 cm annulus at the compressor inlet. Downstream of the compressor exit, a sliding gate valve is used to back-pressure the compressor before the air enters a scroll collector and is exhausted out the side of the facility. The compressor is driven by a 1.04 MW AC motor, of which the output shaft is connected to a 5 : 1 speed-increasing gearbox. An encoder on the motor shaft maintains the shaft speed to within 0.1% of the desired speed.

The compressor geometry is a scaled-up version of the rear stages of a modern high pressure compressor. It operates at engine-representative Reynolds numbers and Mach numbers and has a design corrected speed of 5,000 rpm. The compressor flow path consists of an inlet guide vane (IGV) followed by three stages. The IGV, Stator 1, and Stator 2 rows each have 44 vanes, and Stator 3 has 50. All vanes are NACA-65 series airfoils with circular leading edges. They

Table 1: Summary of stator flow parameters at peak efficiency loading condition.

	Inlet Mach number	Inlet Reynolds number	Solidity	Diffusion factor
Stator 1	0.371	4.34×10^5	1.35	0.464
Stator 2	0.347	4.57×10^5	1.42	0.459

are shrouded and constructed in two monolithic half rings. Knife seals under the hub shroud are used to minimize the leakage flow. O-rings between the casing and the tip shroud prevent any leakage flow in this region. There are 2.38 mm radius fillets at both the tip and the hub. The stator surface roughness is 0.8 μm. Several parameters, including the average inlet Mach number, Reynolds number, solidity, and diffusion factor, for the first two stators at the peak efficiency loading condition are summarized in Table 1. Further details regarding the facility and compressor can be found in [31].

Each vane row is individually indexable allowing the clocking of the vane rows to be changed. For the present study, the IGV and Stator 1 were clocked with respect to Stator 2 and Stator 3. This isolates the clocking changes to the embedded stage. These configurations were defined in terms of a clocking offset (CL) which is the difference between the Stator 1 circumferential position and the Stator 2 circumferential position in terms of a percent vane passage (% vp). Six clocking configurations were used in this study including 0, 15, 32, 49, 66, and 83% vp and are referred to as CL1, CL2, CL3, CL4, CL5, and CL6, respectively. Furthermore, these are the same offsets that have been used in previous vane clocking studies in this facility.

Boundary layer transition at mid-span for Stator 1 will be presented to contrast with the embedded stage results acquired on Stator 2. Then, the measured shear stress on Stator 2 for different clocking positions with respect to Stator 1 will be presented at 20%, 50%, and 75% span. Several loading conditions will be presented.

2.2. Measurement Technique and Analysis. To investigate the boundary layer development on each of the stators including the effects of blade row interactions on boundary layer response, surface-mounted hot-film anemometry was used. Wall shear stress measurements were acquired on the suction surface of all three stators with surface-mounted hot-film anemometry, an established measurement technique to capture unsteady boundary layer development in turbomachinery. The method, originally developed by Bellhouse and Schultz [32], relates the heat transfer of the sensor with the wall shear stress. For the current application, calibration of each sensor is not possible because the one-time-use array is adhered directly to the vane. Using the relation described by Hodson et al. [33], the uncalibrated sensors provide semiqualitative information about the instantaneous state of the boundary layer. This method approximates the heat loss from the substrate to the square of the zero-flow anemometer voltage (E_0). This voltage is acquired both immediately before and immediately after a test. Therefore, wall shear stress can be approximated by the following relation:

$$\tau_w \sim \text{QWSS} = \left(\frac{E^2 - E_0^2}{E_0^2} \right)^3. \quad (1)$$

This quantity is typically referred to as quasi-wall shear stress (QWSS) and will be used to evaluate unsteady boundary layer transition in this research. This method also minimizes effects of sensor-to-sensor variation, allowing for better comparison across an array of sensors.

Boundary layer transition on the vane will be affected by many flow features and geometry parameters, including the inlet Reynolds number, turbulence intensity, surface roughness, overall pressure gradient, leading edge shape, and pressure gradient setup by the curvature of the vane. Many of these flow characteristics change with each stage of a compressor, and thus, acquiring wall-shear stress data on all three stators provides insight to how the boundary layer transition differs from vane to vane through a multistage compressor.

The Stator 2 surface pressure and isentropic Mach number distributions from a CFD solution as well as preliminary wall-shear stress data show that the suction surface flow accelerates around the leading edge up to the position of 20% axial chord. At this position, the peak velocity occurs followed by a nearly constant diffusion rate to the trailing edge. No hot-film sensors will be placed on the pressure side of the airfoil, but the computational results show that the flow decelerates on the pressure surface until around 75% axial chord, after which there is a slight acceleration toward the trailing edge. Based on the vane pressure distribution and a previous test with a coarse ten-sensor array, the distribution of the 18-sensor hot-film array has sensors positioned in the chordwise direction at 4, 8, 12, 16, 20, 24, 28, 32, 36, 40, 44, 48, 52, 56, 60, 70, 80, and 90% Stator 2 suction side length (s), shown in Figure 1. The film substrate, to which the array is mounted, has extra chordwise length near the leading edge so that it can be wrapped around the leading edge terminating on the vane pressure side to avoid tripping the boundary layer on the suction surface. Although the applied film adds approximately 0.006 inches to the vane leading edge thickness and provides a smoother vane surface, vane wake measurements show that it has little effect on the vane's profile loss [34].

A Dantec constant temperature anemometer was used to acquire the surface-mounted hot-film sensor signals. The frequency response of the mounted sensors was determined with a square-wave test at representative flow conditions and was 30 kHz, which is comparable to previous tests with similar sensors. The blade passing frequency of Rotor 1 is 3.0 kHz, 2.75 kHz for Rotor 2, and 2.5 kHz for Rotor 3. Thus, several harmonics of the blade passing frequencies were captured. A study [34] using several overheat ratios was conducted to assess the thermal sensitivity of the sensors

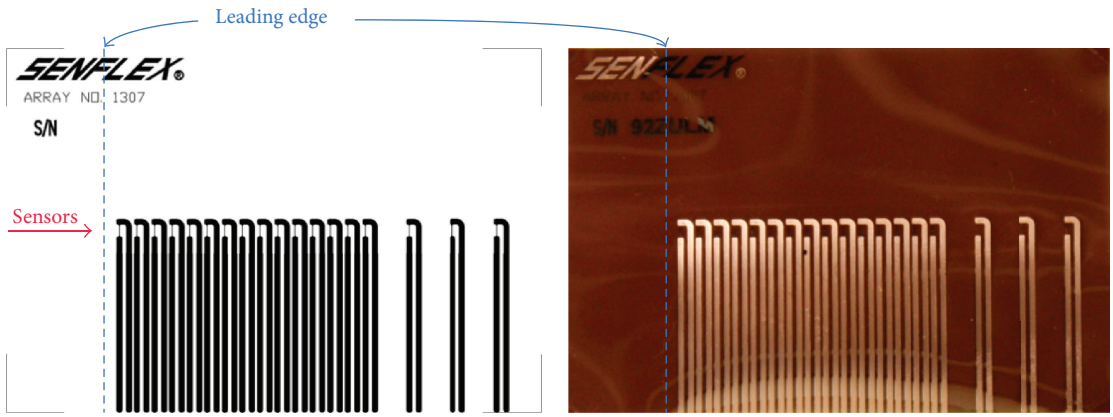

Figure 1: Hot-film sensor array: (a) drawing and (b) photo.

since the compressor has measurable temperature gradients in both the flow field and hardware. From these data, overheat ratios of 1.2 or more provided similar results.

Using a once-per-revolution trigger, the unsteady QWSS data are ensemble-averaged using

$$\langle \mathrm{QWSS}(t) \rangle = \frac{1}{N} \sum_{i=0}^{N-1} \mathrm{QWSS}_i(t), \tag{2}$$

where N is the number of ensembles (500 rotor revolutions for the surface-mounted films). Next, the data are separated into random and periodic fluctuations. The stochastic fluctuations are described by the ensemble averaged root mean square value (RMS), given by

$$\langle \mathrm{RMS}(\mathrm{QWSS}(t)) \rangle = \sqrt{\frac{1}{N} \sum_{i=0}^{N-1} \left(\mathrm{QWSS}_i(t) - \langle \mathrm{QWSS}(t) \rangle \right)^2}. \tag{3}$$

The RMS is normalized by the maximum time-averaged RMS for the rotor revolution at each sensor location. The final statistical quantity used to evaluate the boundary layer development is the skewness. As the third-order moment, skew is a measure of the distribution's symmetry about the mean value:

$$\langle \mathrm{Skew}(\mathrm{QWSS}(t)) \rangle = \frac{1}{N} \sum_{i=0}^{N-1} \left(\mathrm{QWSS}_i(t) - \langle \mathrm{QWSS}(t) \rangle \right)^3. \tag{4}$$

The skew of the surface-mounted hot-film measurements can be used to determine the state of the boundary layer through the transition process. A fully laminar or fully turbulent boundary layer will have a skew near zero. If the boundary layer is mostly laminar with only occasional turbulent fluctuations, then the skew will be positive but small. When the transitional boundary layer becomes more turbulent, with only a small laminar component, the skew becomes negative. Skew is normalized by the maximum time-averaged skew for the entire ensemble averaged revolution. Thus, unsteady vane boundary layer transition can be understood using QWSS, RMS, and skew.

3. Comparison of Mid-Span Boundary Layer Transition for Stator 1 and Stator 2

This section presents the mid-span results of QWSS on Stator 1 and compares them to those at Stator 2, which is part of the embedded stage. The time series of the QWSS data allows for an examination of individual boundary layer disturbances and provides insight to the progress of boundary layer transition. Figure 2 shows time traces of mid-span QWSS for Stator 1 and Stator 2 at the peak efficiency loading condition. For each upstream blade pass period, there is a disturbance in the QWSS. Time has been normalized by the upstream rotor blade passing, thus showing the blade pass period count through a rotor revolution beginning at the once-per-revolution trigger. Near the leading edge for both stators, these are small, discrete influences from each upstream rotor wake passing event. Although the passing of the Rotor 1 wakes creates a clear disturbance by 8.3% s on Stator 1, they grow slowly as they propagate downstream along the suction surface. The convection of one Rotor 1 wake passing is noted by the path labeled A1. The small disturbance of turbulent flow created by the rotor wake does not widen across the entire A1 blade pass period until near 93.2% s.

The Stator 2 boundary layer develops differently despite a similar initial response to the upstream rotor wake passing. Near the leading edge, the small disturbances with each Rotor 2 wake passing are less regular; some blade pass periods appear almost undisturbed, as shown in Figure 2 by comparing path B1 with B2. Each of these grows in strength and width as it propagates downstream through the boundary layer. Around 24–28% s, secondary disturbances between the Rotor 2 wake passing events begin as noted by the dashed line B3. Finally, by 70% s, the individual and secondary disturbances are no longer distinguishable, and the signal consists of increased unsteadiness. These differences in

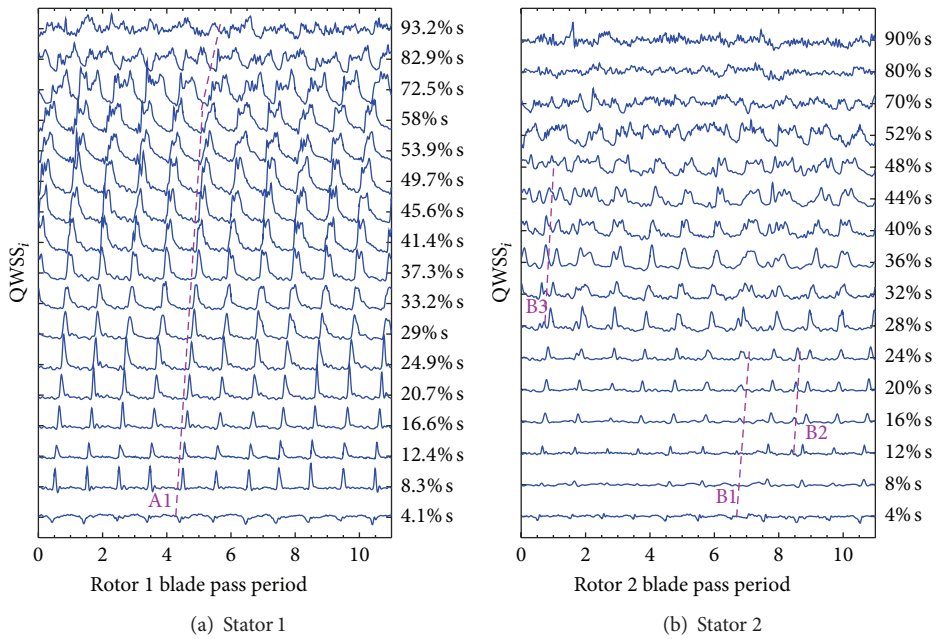

Figure 2: QWSS at peak efficiency: (a) Stator 1 and (b) Stator 2.

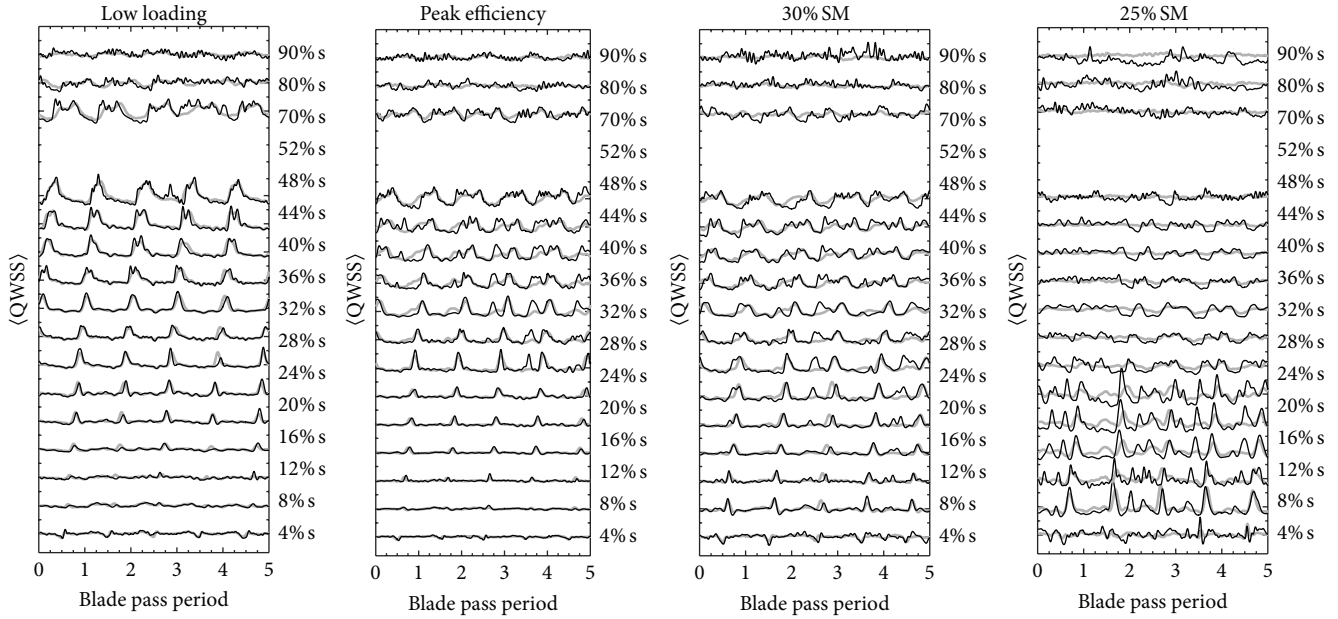

Figure 3: Raw (black) and ensemble-averaged (gray) QWSS for Stator 2 at four loading conditions.

boundary layer disturbance growth and propagation indicate that the Stator 2 boundary layer is transitioning from laminar to turbulent more quickly than Stator 1. The initial smaller or less regular disturbances near the leading edge (4% s) are likely due to the higher inlet turbulence intensity at the Stator 2 inlet, thus allowing the Stator 2 boundary layer to be more resistant to disturbances. However, the embedded environment contains more blade row interactions creating additional disturbances that lead to earlier transition.

The following discussions incorporate ensemble averages of these QWSS data. Figure 3 compares the raw traces from Figure 2 with the ensemble average rotor revolution shown in the thicker grey line for Stator 2 at four loading conditions. Only five blade pass periods are shown. At all loading conditions there are instantaneous disturbances in the thin black line which do not appear in the ensemble-averaged revolution. Boundary layer transition is an unsteady process; wakes are not the only mean by which turbulent behavior can develop along the stator surface. However, the ensemble average indicates the most regular onset location and paths of boundary layer transition. Additionally, in Figure 3, when loading is increased from 30% and 25% SM, there is

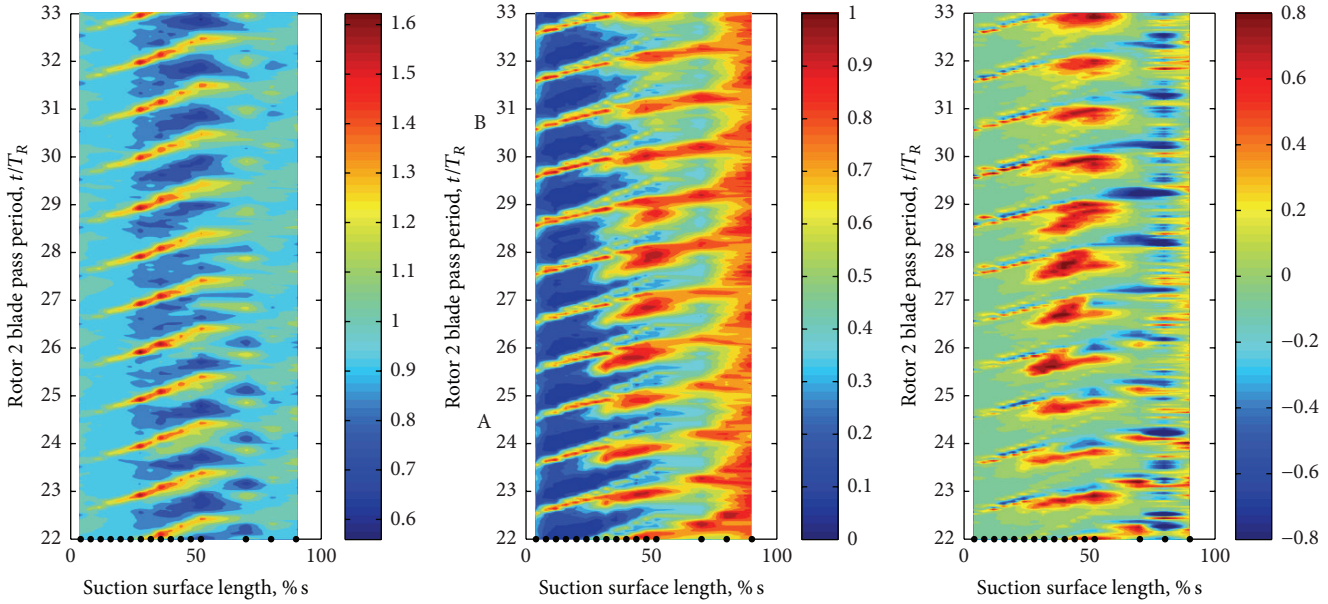

Figure 4: St-diagram of (a) QWSS, (b) RMS, and (c) skew for Stator 2 at peak efficiency loading.

a large shift of the turbulent disturbances toward the leading edge.

Figure 4 shows st-diagrams of QWSS, RMS of QWSS, and skew of QWSS to highlight the different transition paths at mid-span for Stator 2 at the peak efficiency loading condition. The colorbar ranges shown in Figure 4 will be used for all the following st-diagrams. The QWSS clearly defines the wake-induced paths, while RMS and skew are more useful indicators of the transition process. Eleven blade pass periods are shown so that patterns caused by rotor-rotor interactions are included. The QWSS data, shown in Figure 4(a), indicate a clear and repeatable influence from the Rotor 2 wakes. A few of the blade pass periods indicate an additional disturbance in the path between the Rotor 2 wakes, such as the paths that originate near blade pass periods 23, 24, and 25. This additional disturbance is the effect of the Rotor 1 wake. Rotor 1 and Rotor 2 differ in blade count by 3, producing a three-per-revolution pattern; one period of this pattern is shown with eleven Rotor 2 blade pass periods to illuminate these rotor-rotor interactions.

The RMS indicates the unsteadiness that is not phase-locked to the rotor in Figure 4(b). The wake-induced path contains high unsteadiness near the leading edge at each blade pass period, but this is not uniform across the eleven blade pass periods shown. From blade pass periods 22 to 28 (section labeled A) there is low unsteadiness at the 4% s sensor while the wake-induced paths from blade pass periods 28 to 33 (section labeled B) have much higher RMS at 4% s. When considering the path between the wakes, there is also a more notable difference between these sections of the eleven blade pass periods shown in Figure 4. Section A with an additional disturbance in each blade pass period due to the effect of the Rotor 1 wake has much higher RMS that initiates further upstream than the other blade pass periods. The skew values in Figure 4(c) support these observations. In the region where Rotor 1 wakes pass between the Rotor 2 wakes (section A), the skew is near zero at the leading edge in the wake-induced path and does not begin to change until 8% s. Also, the path between the wakes changes to positive skew around 28% s with negative skew by 44% s. Section B where Rotor 1 wakes align with the Rotor 2 wakes has a much stronger effect at the leading edge in the wake-induced path. The RMS is high and the skew contains both positive and negative values at 4% s, while the paths between the wakes do not have high RMS or nonzero skew until approximately 40–44% s.

Therefore, boundary layer transition in the A sector (Rotor 1 wakes between Rotor 2 wakes) is delayed slightly from the leading edge in the Rotor 2 wake-induced path, but in the path between the wakes, transition initiates relatively early. The B section has earlier boundary layer transition in the wake-induced path but later transition in the path between the wakes. In both regions, the Stator 2 boundary layer appears to be nearly separated by 80% s, as indicated by the high unsteadiness and sporadic skew patterns. Furthermore, it is clear that the rotor-rotor interactions are driving the behavior of the boundary layer transition in the path between the wakes. For the remainder of this section the same blade pass periods will be compared between all cases and the effects of rotor-rotor interactions will be addressed with respect to clocking effects.

The boundary layer transitions on Stator 1 and Stator 2 at the peak efficiency loading condition are compared in Figure 5. As suggested with the raw traces of QWSS in Figure 2, Stator 1 boundary layer transition in the wake-induced path is quite similar from one blade pass period to another across the eleven blade pass periods shown in

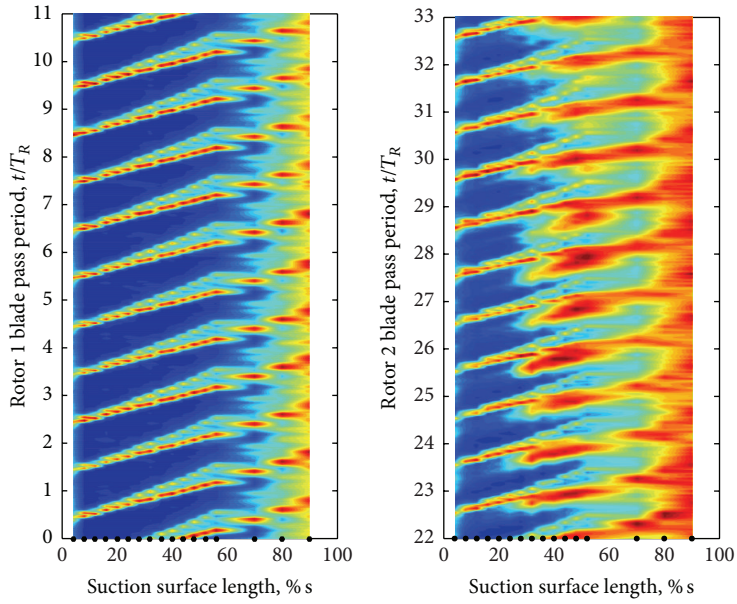

(a) Stator 1 (b) Stator 2

Figure 5: St-diagram of QWSS RMS for (a) Stator 1 and (b) Stator 2, at mid-span for peak efficiency loading.

Figure 5(a). The signal at the leading edge sensor (4% s) contains a strong RMS response at each Rotor 1 blade pass period in the wake-induced path. This path of boundary layer development slowly widens along almost the entire length of the Stator 1 suction surface. The wake-induced path begins to intersect the adjacent wake-induced path between 58% and 72% s. There is no clear secondary path of boundary layer transition between the wake paths. At the 93% s sensor, the boundary layer is fully turbulent and likely beginning to separate, as indicated by the high vales of RMS. Figure 5(b) shows the RMS for Stator 2 (from Figure 4(b)) for direct comparison with Stator 1. The increased level of blade row interactions experienced by Stator 2 just two rows further downstream causes a significantly different transition behavior. The transition path between the wakes is not only present on Stator 2, but it also has high unsteadiness and developments before mid-chord.

The effect of loading condition is shown with st-diagrams of RMS for Stator 2 with four loading conditions in Figure 6. As expected, the vane boundary layer transition moves upstream as loading increases. Generally, the wake-induced paths remain similar with some widening with increased loading. The transition path between the Rotor 2 wakes is strongly affected by the loading condition. In Figure 6(a) for the low loading condition, the transition path between the wakes does not begin until approximately 48% s. At the peak efficiency point (Figure 6(b)) and the following loading at 30% SM (Figure 6(c)), transition between the Rotor 2 wakes has moved to 28% and 24% s, respectively. With a loading increase to 25% SM, the transition path between the wakes shifts even more drastically upstream to 12% s. At loading conditions beyond this point, transition is so far upstream on the vane surface that the st-diagram is no longer useful.

Additionally, there is a shift in the Stator 2 boundary layer separation points between these conditions. The low loading condition in Figure 6(a) shows no sign of boundary layer separation by the last sensor at 90% s. Figures 6(b) and 6(c) both have sporadic, high unsteadiness from 80% s downstream. The 25% SM case in Figure 6(d) has separation occurring by 56% s. These observations are verified with surface flow visualization presented later in the paper.

4. Vane Clocking Effects on the Stator 2 Boundary Layer

Vane clocking is a way to alter the blade row interactions by changing the relative circumferential position of consecutive vane rows with the same vane count. This technique was implemented in this experiment by clocking the IGV and Stator 1 with respect to Stator 2 and Stator 3 resulting in a change in the propagation of the Stator 1 wake with respect to the Stator 2 position. The effects of vane clocking on the Stator 2 boundary layer transition are most clear at the peak efficiency loading condition and the higher loading conditions at 30% and 25% SM, where all stages of the transition process, including both paths of development, are observable.

4.1. Mid-Span Trends. The st-diagrams of RMS and skew are shown in Figure 7 for two clocking configurations at the 30% SM loading condition. Eleven blade pass periods are shown so that the effect of the rotor-rotor interactions can be observed. The transition patterns of these two clocking configurations in Figure 7 are quite different in several ways: the overall RMS level (Figures 7(a) and 7(c)), growth of the wake-induced path, location of the path between the wakes, the influence of rotor-rotor interactions, and location

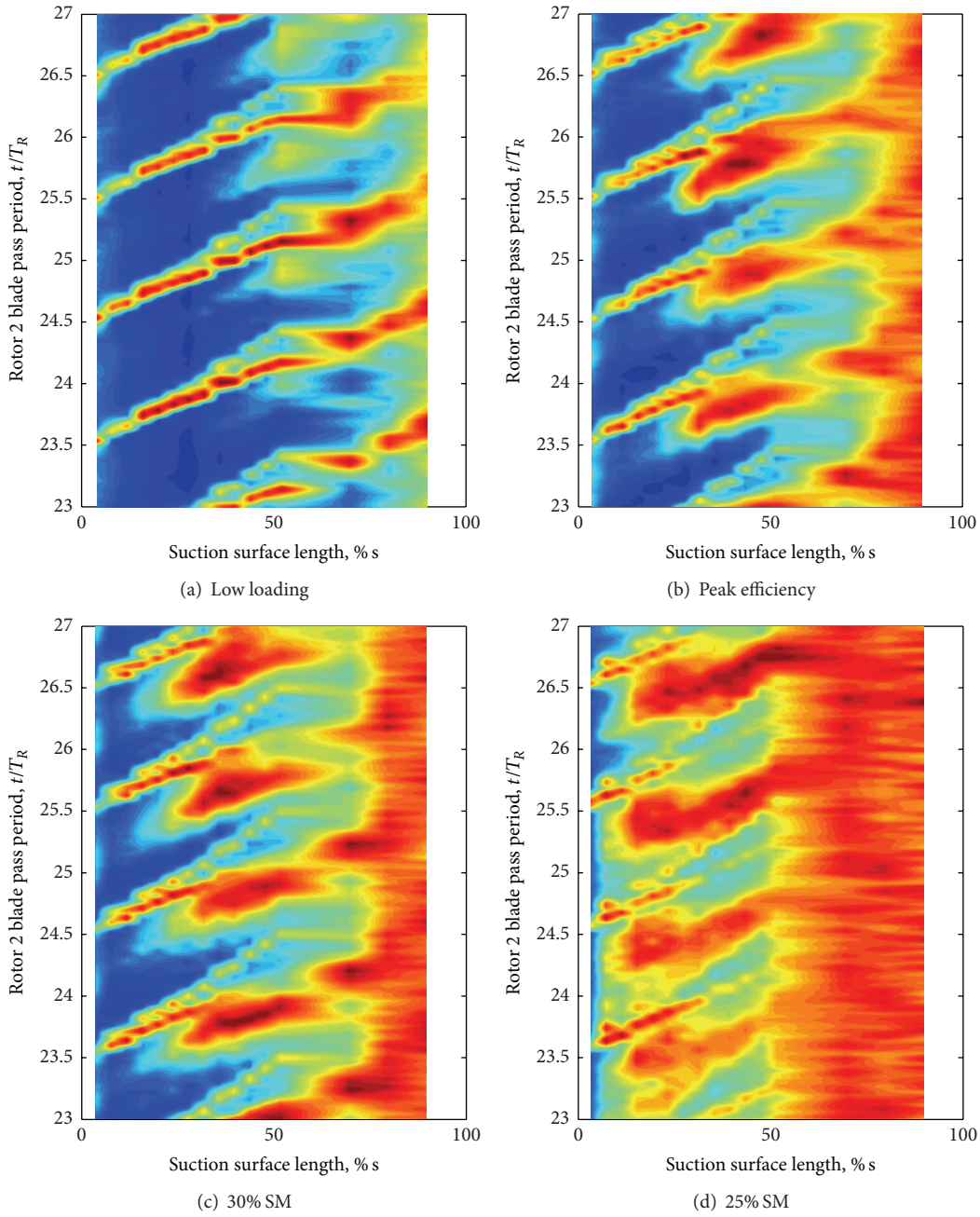

Figure 6: QWSS RMS for mid-span Stator 2 at four loading conditions.

of boundary layer separation. For CL2 in Figures 7(a) and 7(b), the wake-induced paths appear to spread earlier than for CL5 in Figures 7(c) and 7(d), but this could be attributed to interactions with transition between the rotor wake paths. The transition path between the Rotor 2 wakes is more strongly affected by vane clocking. As discussed in earlier sections, transition in the path between the wakes for Stator 2 is strongly governed by the presence of Rotor 1 wake effects and modulates over an eleven-blade pass period. Figure 7 shows that vane clocking has a large influence on the rotor-rotor interactions. For CL2, the Rotor 1 wake interaction is less clear. In general, transition between the wakes is further upstream along the vane surface for this clocking configuration (CL2). In the region where the Rotor 1 wakes are more aligned with the Rotor 2 wakes (blade pass periods 28–33), the wake-induced path appears to widen more quickly and transition between the wakes occurs closer to the leading edge. However, the blade pass periods within 22–25 have a strong boundary layer transition path between the Rotor 2 wake as shown by the high RMS in Figure 7(a) and the clear switch from positive to negative skew in Figure 7(b). The Stator 2 boundary layer behavior has a much stronger response to rotor-rotor interactions for clocking configuration CL5 in Figures 7(c) and 7(d). Transition between the

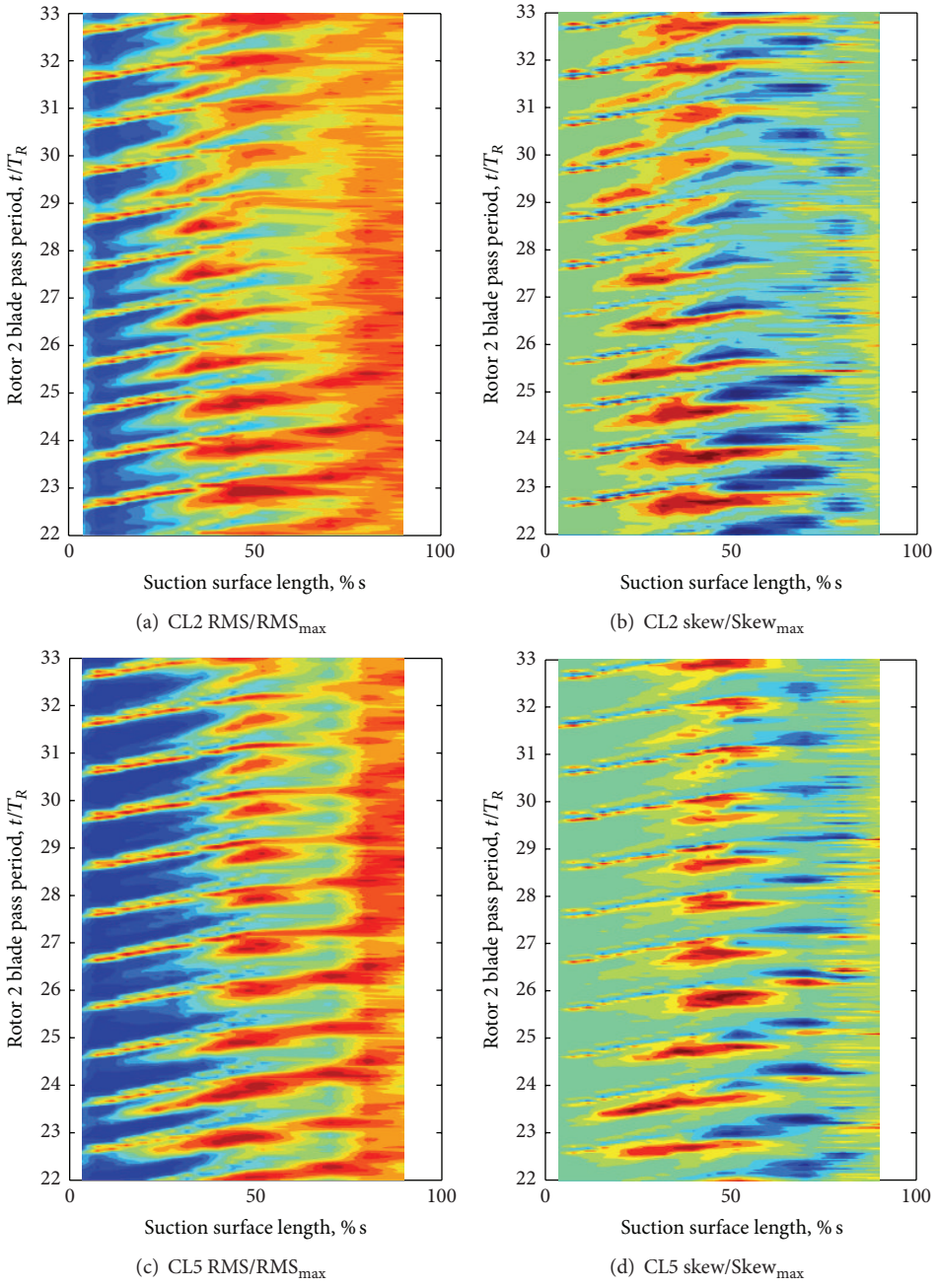

Figure 7: RMS (a, c) and skew (b, d) of Stator 2 QWSS for two clocking configurations at 50% span for 30% SM.

Rotor 2 wakes has a nearly bimodal behavior. From blade pass periods 27 to 32, transition between the Rotor 2 wakes does not occur until approximately 40% s, whereas at blade pass period 23, transition between the wakes is occurring as early as 16% s. Additionally, the CL2 clocking configuration has slightly earlier boundary layer separation around 70% s while clocking configuration CL5 does not have separation until 80% s.

Figure 8 shows total pressure wake profiles acquired at the Stator 2 exit with Kiel-head total pressure rakes. The wake at mid-span for 30% SM and 14% SM is shown in Figures 8(b) and 8(e), respectively. In agreement with the QWSS results, clocking configuration CL2 has a wider wake and more total pressure loss than CL5. As loading is increased, the difference in total pressure loss between clocking configurations does not change significantly at mid-span. The wake profiles at the hub and tip endwalls are also shown in Figures 8(a), 8(c), 8(d), and 8(f) and are discussed in the next section.

A Fourier analysis is used to provide an estimate of the locations of transition along the vane surface. Since vane clocking is significantly altering the transition between the wakes, the FT magnitudes at the Rotor 1 blade passing frequencies along the Stator 2 surface are shown in Figure 9 for six clocking configurations. There is a clear streamwise shift

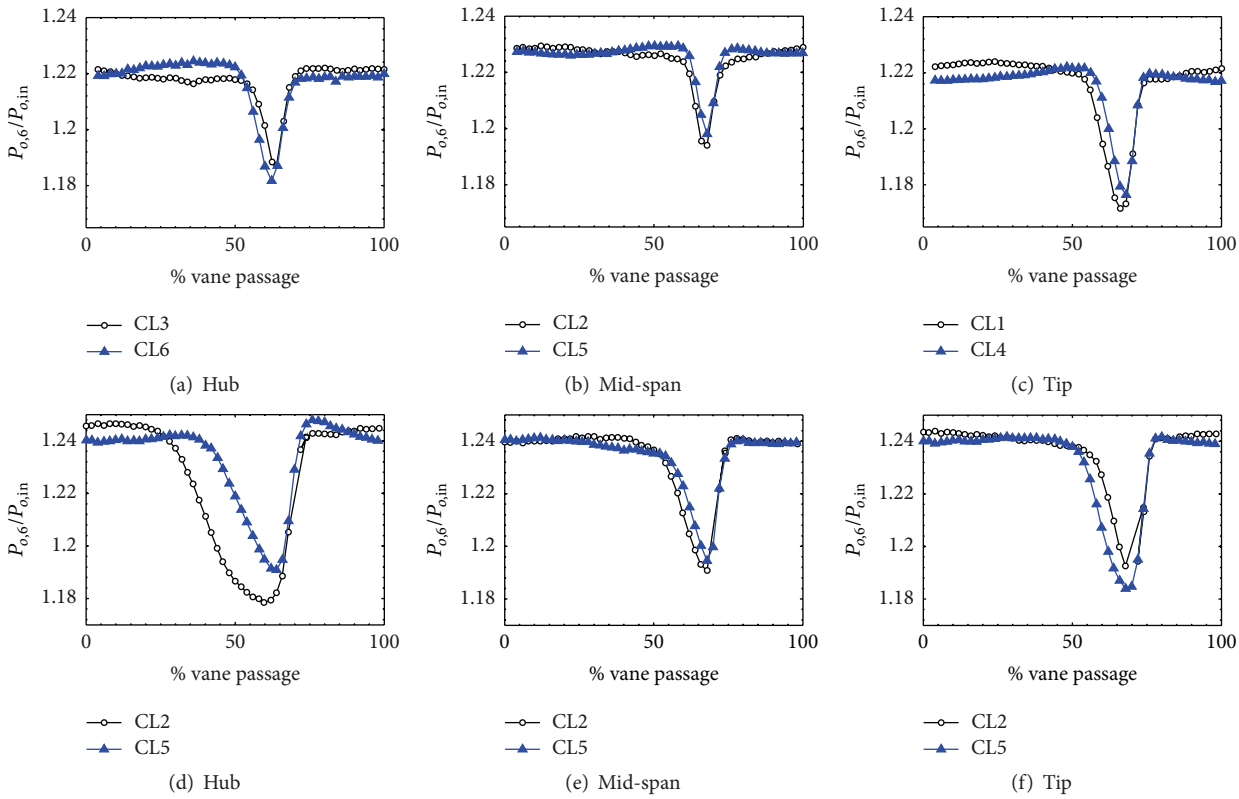

Figure 8: Stator 2 wakes near the peak efficiency loading (30% SM) for (a) hub, (b) mid-span, and (c) tip region, and at a high loading condition (14% SM) for the (d) hub, (e) mid-span, and (f) tip.

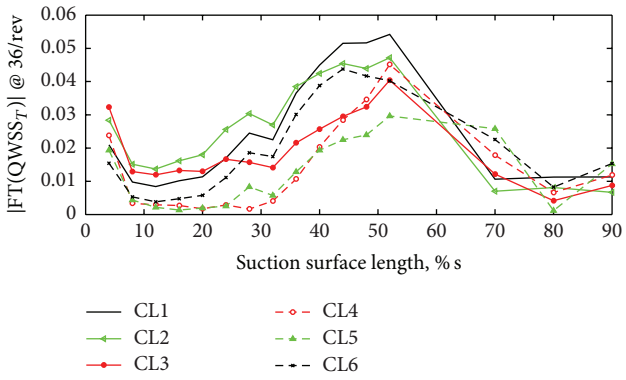

Figure 9: Magnitude of FT at Rotor 1 blade passing frequency for six clocking configurations.

in transition with clocking configuration. The configurations shown in Figure 7 (CL2 and CL5) are the bounding cases. Transition between the wakes begins at approximately 20% s for CL2 and 32% for CL5.

Surface flow visualization was used to identify boundary layer separations on the vane suction sides. The technique uses a mixture of powered paint and kerosene (1 : 2.5) that is injected at the inlet of the compressor. The kerosene evaporates and the paint is deposited in regions of recirculation on the vanes. Further details on the measurement technique may be found in [33]. Figure 10 shows images of the Stator 2 suction side viewed from the trailing edge with flow from left to right for three loading conditions, low loading, peak efficiency, and a high loading at 17% SM. For comparison with the QWSS data, the boundary layer separation occurring at 50% span in these images must be considered. At the low loading condition shown in Figure 10(a), the hub and tip corner separations do not meet and the flow is attached at the trailing edge near 50% span and corresponds well with the RMS in Figure 6(a). In Figure 10(b), the corner separations have met and the boundary layer is separated by about 80% s. The high loading condition shown in Figure 10(c) is a little higher (17% SM) than the condition in Figure 6(d) (25% SM) but shows how drastically the corner separations grow with increased loading. More separation line images and changes in steady total pressure loss with loading for Stator 1 can be found in [35].

4.2. Endwall Trends. The secondary flow along the casing and hub endwall caused by the cross-flow pressure gradient interacts with the already weak boundary layer on the vane suction surface enhancing the adverse environment for boundary layer development. This promotes earlier boundary layer transition and a complex three-dimensional flow separation, often called a corner separation. The hot-film data acquired at a spanwise location both near the hub (20% span) and the tip (75% span) reflect this behavior and are presented here.

In the tip region, boundary layer transition occurs further upstream along the vane surface near the endwall as

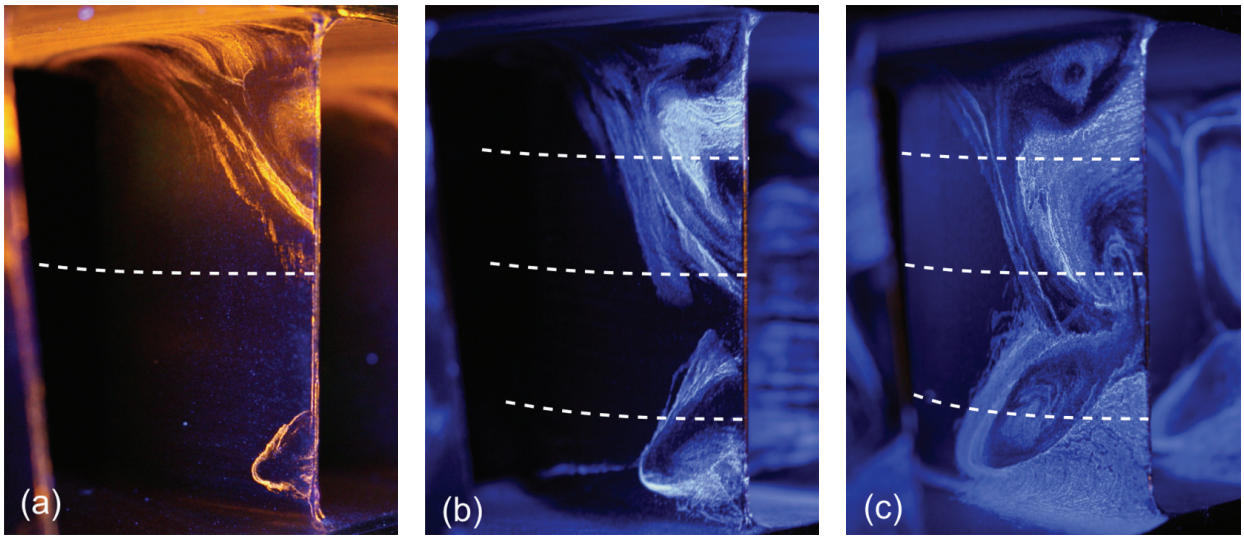

Figure 10: Flow visualization of vane boundary layer separations along Stator 2 suction surface at three loading conditions: (a) low loading, (b) peak efficiency, and (c) 17% SM high loading.

anticipated from the flow visualization images indicating the presence of corner separations. Figure 11 shows eleven blade pass periods of QWSS RMS and skew for two clocking configurations (CL1 and CL4) at the peak efficiency loading condition (33% SM). Compared to the mid-span data presented in Figure 6(c), the peak values of RMS are much further upstream along the vane surface. This can also be observed by comparing with the contours of skew at 50% span (30% SM) from Figures 7(b) and 7(d). The Stator 2 boundary layer is already undergoing the transition process at the leading edge. Differences in the influence of Rotor 1-Rotor 2 interactions on the Stator 2 boundary layer transition process are present in Figure 11. For clocking configuration CL4, transition is completed further upstream along the vane surface during blade pass periods 23–27, whereas there is essentially no change in transition location between different blade pass periods for clocking configuration CL1.

Additionally, in the tip region (75% span), clocking configuration CL1 has wider, stronger Rotor 2 wake-induced paths compared to CL4 due to the presence of the tip leakage flow alongside the incoming Rotor 2 wake. This is due to a difference in inlet conditions from upstream blade row interactions, as shown by previous studies [17]. Clocking configuration CL1 has a larger region of unsteadiness penetrating further radially at the Stator 2 leading edge compared to CL4 due to the Stator 1 wake-Rotor 2 tip leakage flow interaction. This influence of the wider wake-induced path results in earlier transition and separation for CL1. Furthermore this affects the total pressure loss across Stator 2. Figure 8(c) shows the Stator 2 wakes in the tip region for CL1 and CL4 at the peak efficiency loading condition. Clocking configuration CL1 has slightly wider wakes at the tip endwall. As loading is increased, transition occurs near the leading edge making distinctions in the details of wake-boundary layer interactions difficult to distinguish because there are no longer transition paths. Stator wakes from steady total pressure traverses at high loading conditions shown in Figure 8(f) are thicker supporting the QWSS data and the flow visualization that indicates earlier boundary layer separation. Furthermore, the differences in boundary layer separation between clocking configurations are enhanced at these conditions, especially due to the contribution of the endwall to the corner separation.

The QWSS data acquired at the hub utilized the coarser hot-film array from a previous study [30, 34]. Similar to the tip, in the hub region, the loading conditions closer to peak efficiency provide some details about the differences in boundary layer development between clocking configurations. At the near peak efficiency loading condition (30% SM) the boundary layer has transitional behavior near the leading edge, as shown in Figure 12 with the QWSS skew for clocking configurations CL3 and CL6. Transition is complete by 50% s and separation occurs near 75–80% s. The flow visualization in Figure 10(b) supports these results at 20% span. The influence of Rotor 1-Rotor 2 interactions changes slightly between the clocking configurations, but these changes are less than the changes observed at the other spanwise locations. Figure 12 also reveals some differences in the transition process between the two clocking configurations. In configuration CL3, there is more positive skew near the leading edge, but the following region of negative skew is smaller than clocking configuration CL6. The boundary layer separation occurs at roughly the same chordwise location for these two clocking configurations near peak efficiency. This is also supported with Stator 2 wake profiles in Figure 8(a), in which CL6 has a slightly wider wake.

At the high loading condition (not shown), there is no indication of transitional flow on the Stator 2 suction side near the hub (20% span). The flow visualization shows the large increase in hub corner separation size between peak efficiency and high loading (17% SM) in Figures 10(b) and 10(c). The QWSS data do contain some frequency content

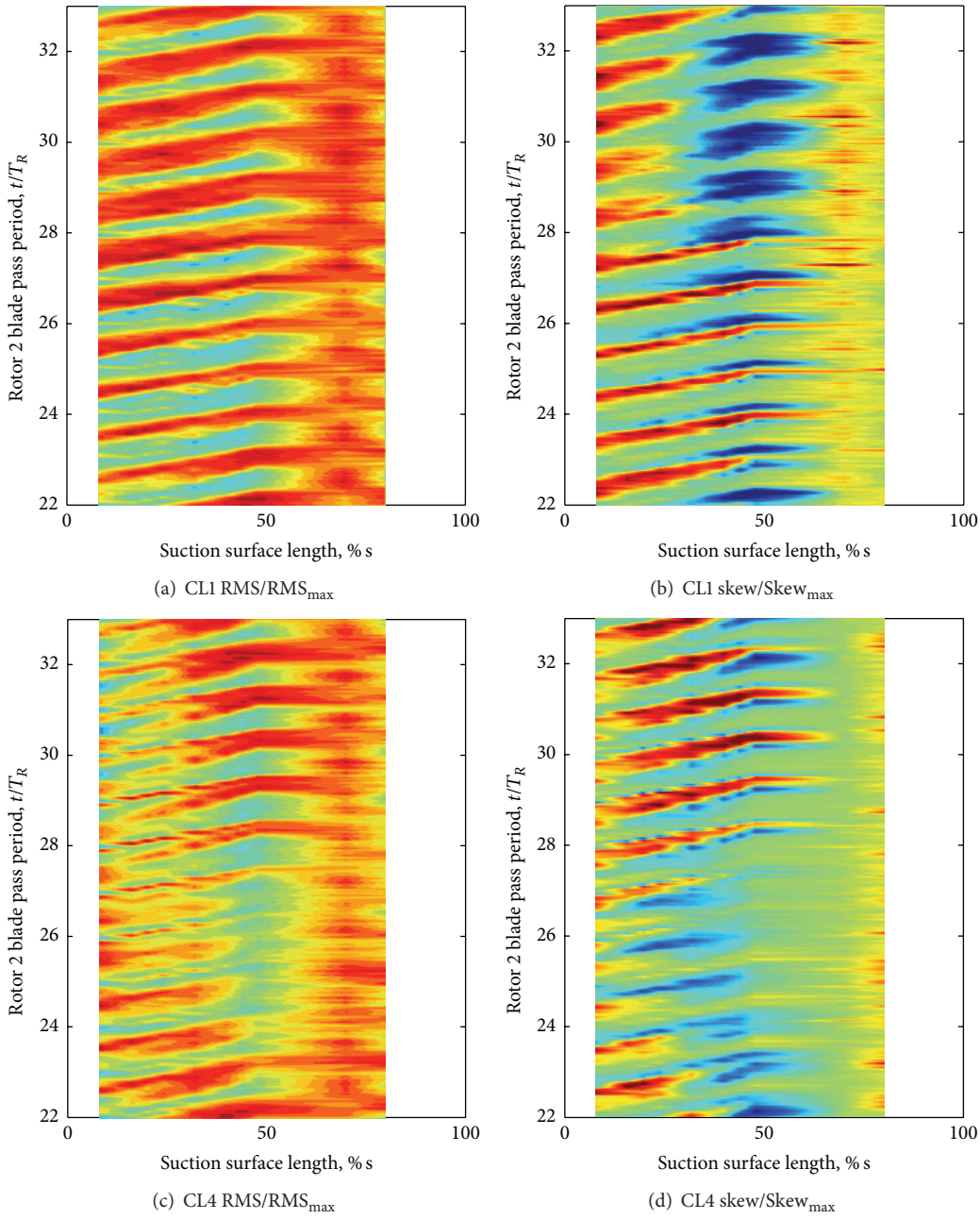

Figure 11: RMS (a, c) and skew (b, d) of Stator 2 QWSS for two clocking configurations at 75% span for 33% SM.

related to the upstream rotor blade passing frequencies which show differences between clocking configurations associated with the Rotor 1-Rotor 2 interactions. The high loss (wide Stator 2 wakes) clocking configuration, CL2, has less of the 3/rev beating pattern and this more defined Rotor 2 wake influence at the leading edge. The QWSS data show that CL2 has earlier boundary layer separation at high loading, but the difference is not as drastic as the wakes downstream of the Stator 2 hub suggest in Figure 8(d). The wake size near the endwall at the high loading conditions is also governed by the size of the corner separation. Therefore, the separation along the vane surface (as measured in this study), as well as the boundary layer separation on the endwall, contributes to the wake size.

5. Conclusions

Wall shear stress data were acquired on Stator 1 and Stator 2 in the Purdue Three-Stage Axial Compressor at several loading conditions. An array of 18 surface-mounted hot-film sensors was used at 50% span for each vane row and 75% span on Stator 2. An array of 10 surface-mounted hot-film sensors was used at 20% span on Stator 2. Statistical and Fourier analyses were used to evaluate to boundary layer development.

Boundary layer transition along Stator 1 and Stator 2 suction surfaces is markedly different due to the difference in upstream blade row interactions for the two vane rows. Boundary layer transition on Stator 1 occurs further downstream on the vane and the wake-induced paths from one

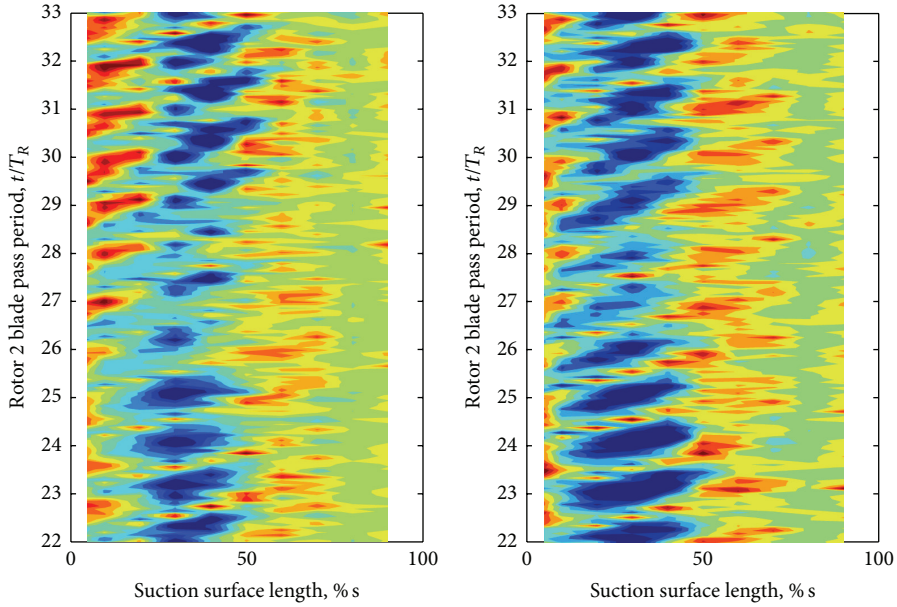

(a) CL3 skew/Skew$_{max}$ (b) CL6 skew/Skew$_{max}$

FIGURE 12: Skew for clocking configurations: (a) CL3 and (b) CL6 at 20% span for 30% SM loading.

Rotor 1 wake to the next are nearly indistinguishable. On the other hand, rotor-rotor interactions shift the location of transition in the path between the wakes for Stator 2. Generally, when the further upstream rotor wake is present between the primary incoming rotor wakes, transition moved upstream on the vane. This shift in boundary layer transition onset location was as large as 15% s. These interactions account for approximately half the blade to blade variability and up to three-quarters of the variability in the transition region.

The effects of vane clocking on transition of the second stator were considered by clocking the IGV and Stator 1 through six clocking configurations with respect to Stator 2. This had a profound effect on the transition behavior, particularly for the path between the wakes, as presented at mid-span. The clocking configuration CL2 had earlier transition in the path between the wakes by approximately 12% s and the wake-induced path widen more quickly, which could be due to influences from the path between the wakes. Also for clocking configuration CL2, the 3/rev modulation was less pronounced. The clocking configuration half a vane passage out of phase experienced a strong modulation of the path between the wakes due to rotor-rotor interactions. This difference in transition onset across this pattern was 24% s. In the endwall regions (hub and tip), the Stator 2 boundary layer transition occurred much closer to the leading edge compared to mid-span at the same loading condition. Near the tip at 75% span, the CL1 clocking configuration had wider Rotor 2 wake-induced paths due to the effect of the rotor tip leakage flow. This same behavior was not observed at other clocking configurations because the Stator 2 inlet conditions vary with clocking configuration due to the Stator 1 wake-Rotor 2 tip leakage flow interaction. These results show the compounding effect blade row interactions can have on boundary layer development and further motivate the need for computational codes to capture these effects.

Nomenclature

CL: Clocking configuration
E: Anemometer voltage
N_c: Corrected speed
P_o: Total pressure
QWSS: Quasi-wall shear stress
R: Rotor
RMS: Root mean square
S: Stator
SM: Stall margin.

Competing Interests

The authors declare that they have no competing interests.

Acknowledgments

The authors would like to thank Rolls-Royce for the permission to publish this work.

References

[1] J. J. Adamczyk, "Model equation for simulating flows in multistage turbomachinery," ASME Paper 85-GT-226. (NASA TM-86869), 1984.

[2] J. J. Adamczyk, R. A. Mulac, and M. L. Celestina, "A model for closing the inviscid form of the average-passage equation system," ASME Paper 86-GT-227, NASA, 1986.

[3] K. C. Hall, J. P. Thomas, and W. S. Clark, "Computation of unsteady nonlinear flows in cascades using a harmonic balance technique," *AIAA Journal*, vol. 40, no. 5, pp. 879–886, 2002.

[4] J. M. Verdon, "Review of unsteady aerodynamic methods for turbomachinery aeroelastic and aeroacoustic applications," *AIAA Journal*, vol. 31, no. 2, pp. 235–250, 1993.

[5] L. Castillon, G. Billinnet, J. Riou, S. Peron, and C. Benoit, "A technological effect modeling on complex turbomachinery applications with an overset grid numerical method," *Journal of Turbomachinery*, vol. 136, no. 10, Article ID 101005, 2014.

[6] Y. K. P. Shum, C. S. Tan, and N. A. Cumpsty, "Impeller-diffuser interaction in a centrifugal compressor," *Journal of Turbomachinery*, vol. 122, no. 4, pp. 777–786, 2000.

[7] R. J. Miller, R. W. Moss, R. W. Ainsworth, and C. K. Horwood, "Time-resolved vane-rotor interaction in a high-pressure turbine stage," *Journal of Turbomachinery*, vol. 125, no. 1, pp. 1–13, 2003.

[8] W. S. Barankiewicz and M. D. Hathaway, "Effects of stator indexing on performance in a low speed multistage axial compressor," ASME Paper 97-GT-496, 1997.

[9] G. J. Walker, J. D. Hughes, I. Köhler, and W. J. Solomon, "The influence of wake-wake interactions on loss fluctuations of a downstream axial compressor blade row," ASME Paper 97-GT-469, ASME, 1997.

[10] V. E. Saren, N. M. Savin, D. J. Dorney, and R. M. Zacharias, "Experimental and numerical investigation of unsteady rotor-stator interaction on axial compressor stage (with IGV) performance," in *Unsteady Aerodynamics and Aeroelasticity of Turbomachines, Proceedings of the 8th International Symposium, Stockholm, Sweden, 14–18 September 1997*, pp. 407–424, Springer, 1998.

[11] N. L. Key, P. B. Lawless, and S. Fleeter, "An experimental study of vane clocking effects on embedded compressor stage performance," *Journal of Turbomachinery*, vol. 132, no. 1, Article ID 011018, 10 pages, 2010.

[12] S. T. Hsu and A. M. Wo, "Reduction of unsteady blade loading by beneficial use of vortical and potential disturbances in an axial compressor with rotor clocking," *Journal of Turbomachinery*, vol. 120, no. 4, pp. 705–713, 1998.

[13] R. Mailach and K. Vogeler, "Aerodynamic blade row interactions in an axial compressor-part 2: unsteady profile pressure distribution and blade forces," *Journal of Turbomachinery*, vol. 126, no. 1, pp. 45–51, 2004.

[14] G. J. Walker and A. R. Oliver, "The effect of interaction between wakes from blade rows in an axial flow compressor on the noise generated by blade interaction," *Journal of Engineering for Power*, vol. 94, no. 4, pp. 241–248, 1972.

[15] D. P. Schmidt and T. H. Okiishi, "Multistage axial-flow turbomachine wake production, transport, and interaction," *AIAA Journal*, vol. 15, no. 8, pp. 1138–1145, 1977.

[16] S. Kamiyoshi and S. Kaji, "Tone noise reduction of multi-stage fan by airfoil clocking," AIAA Paper 2000-1992, 1992.

[17] N. R. Smith, W. L. Murray III, and N. L. Key, "Considerations for measuring compressor aerodynamic excitations including rotor wakes and tip leakage flows," *Journal of Turbomachinery*, vol. 138, no. 3, Article ID 031008, 9 pages, 2016.

[18] K. L. Gundy-Burlet and D. J. Dorney, "Physics of airfoil clocking in axial compressors," ASME Paper 97-GT-444, 1997.

[19] N. R. Smith and N. L. Key, "Vane clocking effects on stator loss for different compressor loading conditions," *Journal of Propulsion and Power*, vol. 31, no. 2, pp. 519–526, 2015.

[20] N. R. Smith and N. L. Key, "Vane clocking effects on stall margin in a multistage compressor," *Journal of Propulsion and Power*, vol. 29, no. 4, pp. 891–898, 2013.

[21] D. J. Dorney, O. P. Sharma, and K. L. Gundy-Burlet, "Physics of airfoil clocking in a high-speed axial compressor," ASME Paper 98-GT-82, 1998.

[22] L. Müller, R. Mailach, K. Vogeler, H. Jia, and G. Xi, "Unsteady blade loading with clocking in multistage axial compressors, part 2," *Journal of Propulsion and Power*, vol. 26, no. 1, pp. 36–45, 2010.

[23] L. W. Griffin, F. W. Huber, and O. P. Sharma, "Performance improvement through indexing of turbine airfoils: part 2—numerical simulation," *Journal of Turbomachinery*, vol. 118, no. 4, pp. 636–642, 1996.

[24] N. R. Smith and N. L. Key, "Effects of blade row interactions on unsteady stator surface pressures in an embedded compressor stage," in *Proceedings of the 22nd International Symposium on Air Breathing Engines*, ISABE-2015-20104, Phoenix, Ariz, USA, October 2015.

[25] G. J. Walker, J. D. Hughes, and W. J. Solomon, "Periodic transition on an axial compressor stator: incidence and clocking effects: part I—experimental data," *Journal of Turbomachinery*, vol. 121, pp. 398–407, 1999.

[26] A. D. Henderson, G. J. Walker, and J. D. Hughes, "The influence of turbulence on wake dispersion and blade row interaction in an axial compressor," in *Proceedings of the ASME Turbo Expo: Power for Land, Sea, and Air*, Paper no. GT2005-68432, pp. 1323–1333, Reno, Nev, USA, June 2005.

[27] J. Städing, J. Friedrichs, T. Waitz, and C. Dobriloff, "The potential of rotor an stator clocking in a 2.5-stage low-speed axial compressor," in *Proceedings of teh ASME Turbo Expo 2012: Turbine Technical Conference and Exposition*, Paper no. GT2012-68353, Copenhagen, Denmark, June 2012.

[28] D. E. Halstead, D. C. Wisler, T. H. Okiishi, G. J. Walker, and H. P. Hodson, "Boundary layer development in axial compressors and turbines: parts 1–4," *Transactions of the ASME Journal of Turbomachinery*, vol. 119, no. 1, pp. 114–127, 1997.

[29] R. Mailach and K. Vogeler, "Aerodynamic blade row interactions in an axial compressor—part I: unsteady boundary layer development," *Journal of Turbomachinery*, vol. 126, no. 1, pp. 35–44, 2004.

[30] N. R. Smith and N. L. Key, "Unsteady vane boundary layer response to rotor-Rotor interactions in a multistage compressor," *Journal of Propulsion and Power*, vol. 30, no. 2, pp. 416–425, 2014.

[31] J. R. Brossman, N. R. Smith, A. Talalayev, and N. L. Key, "Tailoring inlet flow to enable high accuracy compressor performance measurements," *International Journal of Turbo and Jet Engines*, vol. 28, no. 4, pp. 309–320, 2011.

[32] B. J. Bellhouse and D. L. Schultz, "Determination of mean and dynamic skin friction, separation and transition in low-speed flow with a thin-film heated element," *Journal of Fluid Mechanics*, vol. 24, no. 2, pp. 379–400, 1966.

[33] H. P. Hodson, I. Huntsman, and A. B. Steele, "An investigation of boundary layer development in a multistage LP turbine," *Journal of Turbomachinery*, vol. 116, no. 3, pp. 375–383, 1994.

[34] N. R. Smith, *Experimental investigation of vane clocking effects on stall performance and unsteady van boundary layer development in a multistage compressor [M.S. thesis]*, School of Aeronautics and Astronautics, Purdue University, West Lafayette, Ind, USA, 2011.

[35] N. R. Smith and N. L. Key, "Flow visualization for investigating stator losses in a multistage axial compressor," *Experiments in Fluids*, vol. 56, article 94, 2015.

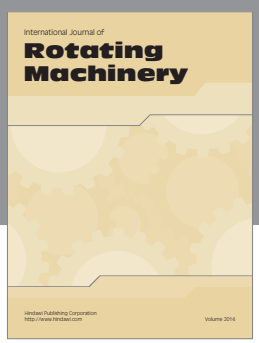

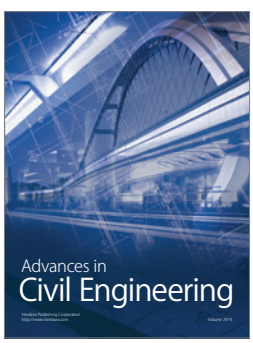

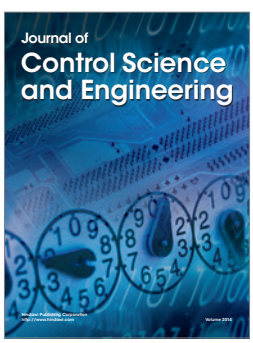

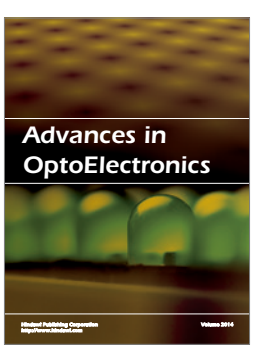

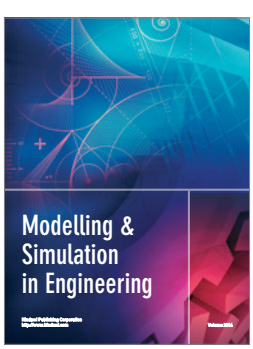

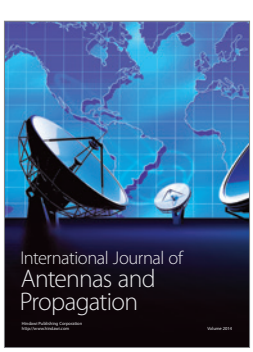

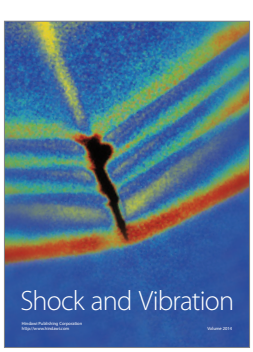

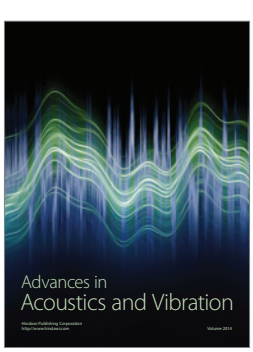

Hindawi

Submit your manuscripts at
http://www.hindawi.com